Electronic supplementary information (ESI) for

Biomass-derived polyol esters as sustainable phase change materials for renewable energy storage

Magdalena Gwóźdź,[a] Marta Markiewicz,[b] Stefan Stolte,[b] Anna Chrobok,[a] David R. Turner,[c] Karolina Matuszek,[*c] and Alina Brzęczek-Szafran[*a]

Correspondence to: Karolina.Matuszek@monash.edu, Alina.Brzeczek-Szafran@polsl.pl

List of contents

List of figures

List of tables

Materials and methods

Materials

The long-chain sugar acid esters of L-(+)-Tartaric acid (>99.5%) were synthesized using 1-dodecanol (>98%), 1-hexadecanol (>99%), 1-octadecanol (>99%), and 1-docanozol (>99%) from Sigma-Aldrich. The reaction also used AmberlystTM-15 catalyst commercially available from Merck. Ethanol was used for crystallization to purify the final product of the synthesis. The all reagents were used without purification.

General procedure of synthesis diesters derivatives of L-(+) tartaric acid

L-(+)-tartaric acid (0.5 g, 3.44 mmol), fatty alcohol (5 g, 0,0019 mol) and Amberlyst 15 (1.5 g) were combined in a round-bottom flask. The reaction mixture was stirred at 70°C for 24 hours. After the reaction was completed, 40 ml ethanol was added and the mixture was heated to dissolve the product. The Amberlyst 15 was separated by hot filtration. After cooling to room temperature, the crude product crystallized immediately and was filtered off, followed by recrystallization from ethanol (30 ml).

(R, R)-di-n-dodecyltartrate

$C_{28}H_{52}O_4$; 452.39 g mol^{-1}. Yield: 65%; white powder; mp = 67 °C (lit. 64–66 °C[1])

^{1}H NMR (400 MHz, $CDCl_3$) δ 4.52 (d, *J* = 6.0 Hz, 2H), 4.26 (td, *J* = 6.8, 3.1 Hz, 4H), 3.15 (d, *J* = 7.1 Hz, 2H), 1.68 (dt, *J* = 8.1, 6.5 Hz, 4H), 1.41 – 1.20 (m, 32H), 0.92 – 0.82 (m, 6H).

^{13}C NMR (101 MHz, $CDCl_3$) δ 171.65, 77.23, 72.03, 66.64, 31.92, 29.63, 29.56, 29.48, 29.35, 29.18, 28.52, 25.73, 22.69, 14.12.

ESI-MS: $[M+H]^+$ calcd.: 487.3999; found: 487.3996,

(R, R)-di-n-hexadecyltartrate

$C_{36}H_{70}O_6$; 598.948 g mol^{-1}. Yield: 68%; white powder; mp = 77 °C (lit. 78–79 °C[1])

^{1}H NMR (400 MHz, $CDCl_3$) δ 4.52 (s, 2H), 4.26 (td, *J* = 6.8, 3.2 Hz, 4H), 1.68 (dt, *J* = 8.1, 6.6 Hz, 4H), 1.26 (s, 52H), 1.00 – 0.71 (m, 6H).

^{13}C NMR (101 MHz, $CDCl_3$) δ 170.61, 76.19, 70.96, 65.63, 30.91, 28.67, 28.64, 28.61, 28.54, 28.46, 28.35, 28.16, 27.49, 24.70, 21.68, 13.11.

ESI-MS: $[M+H]^+$calcd.: 599.5251; found: 599.5238, $[M+Na]^+$ calcd.: 621.5070; found: 621.5069

(R, R)-di-n-octadecyltartrate

$C_{40}H_{78}O_6$; 655.056 g mol^{-1}. Yield: 70%; white powder; mp = 82 °C

^{1}H NMR (400 MHz, $CDCl_3$) δ 4.45 (s, 2H), 4.18 (tt, *J* = 7.0, 3.5 Hz, 4H), 3.04 (s, 2H), 1.62 (p, *J* = 6.8 Hz, 4H), 1.19 (s, 50H), 0.81 (t, *J* = 6.8 Hz, 6H).

^{13}C NMR (101 MHz, $CDCl_3$) δ 170.62, 76.19, 70.98, 65.62, 30.91, 28.68, 28.65, 28.62, 28.55, 28.46, 28.35, 28.16, 27.49, 24.70, 21.68, 13.11.

ESI-MS: $[M+H]^+$ calcd.:655.5876 ; found: 656.5861, $[M+Na]^+$ calcd.: 678.5690, found: 678.5693

(R, R)-di-n-docanosyltartrate

$C_{48}H_{94}O_6$; 767.3 g mol^{-1}. Yield: 60%; white powder; mp = 94 °C

^{1}H NMR (400 MHz, $CDCl_3$) δ 4.52 (s, 2H), 4.26 (td, *J* = 6.7, 3.2 Hz, 4H), 1.69 (dq, *J* = 8.0, 6.6 Hz, 4H), 1.26 (s, 76H), 0.93 – 0.79 (m, 6H).

^{13}C NMR (101 MHz, $CDCl_3$) δ 171.65, 77.23, 72.02, 66.65, 31.94, 29.72, 29.69, 29.68, 29.65, 29.58, 29.50, 29.38, 29.19, 28.53, 25.73, 22.71, 20.53, 14.13.

ESI-MS: $[M+Na]^+$ calcd.: 789.6948; found: 789.6944

General procedure of synthesis diesters derivatives of mucic acid

In a round-bottom flask, mucic acid dibutyl ester (which was described according to the literature)[2] (22.5 g, 0.15 mol), fatty alcohol (30 g, 0.41 mol), and p-toluenesulfonic acid (1.5 g, 5 mol% MA) as a catalyst were subjected to reflux for 24 hours. After cooling, the n-butanol was added. The resulting residue was then filtered and subjected to recrystallization from water and next from THF or pyridine, yielding a white powder.

Di-n-dodecylmucate

$C_{38}H_{74}O_8$; 658.5 g mol^{-1}, Yield: 52%; white powder; mp = 137 °C

^{1}H NMR (400 MHz, DMSO) δ 4.92 – 4.63 (m, 4H), 4.29 (d, *J* = 7.7 Hz, 2H), 4.05 (d, *J* = 8.2 Hz, 4H), 1.58 (d, *J* = 8.1 Hz, 4H), 1.24 (s, 18H), 0.98 – 0.75 (m, 6H).

ESI-MS: $[M+Na]^+$ calcd.: 681.5261 ; found: 681.5178

Di-n-octadecylmucate

$C_{42}H_{82}O_8$; 714.6 g mol^{-1}, Yield: 40%; white powder; mp = 124 °C

^{1}H NMR (400 MHz, DMSO) δ 4.77 (dd, J = 20.2, 11.2 Hz, 4H), 4.24 (t, J = 9.1 Hz, 2H), 4.12 – 3.92 (m, 4H), 3.74 (s, 2H), 1.54 (m, 4H), 1.19 (m, 50H), 0.92 – 0.73 (m, 6H).

ESI-MS: $[M+Na]^+$ calcd.: 737.5908; found: 737.5419

NMR spectra

Tartaric acid series

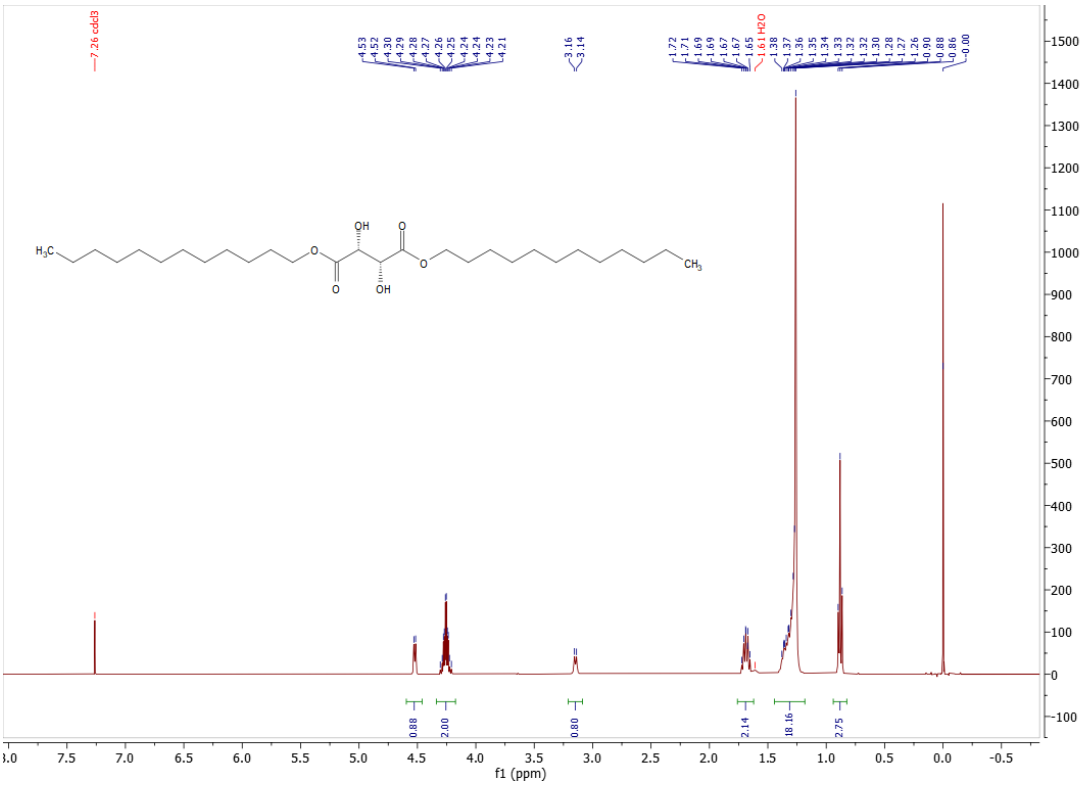

Figure S 1 ^{1}HNMR spectrum of (R,R)-di-n-dodecyltartrate

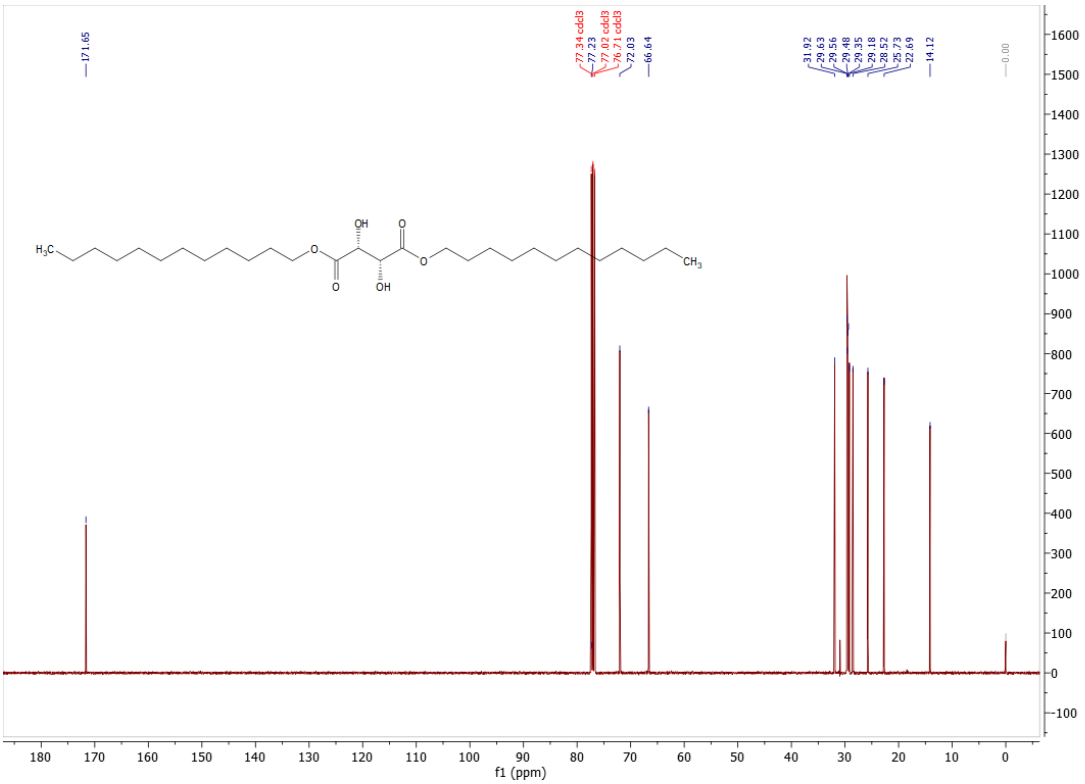

Figure S 2 ^{13}CNMR spectrum of (R,R)-di-n-dodecyltartrate

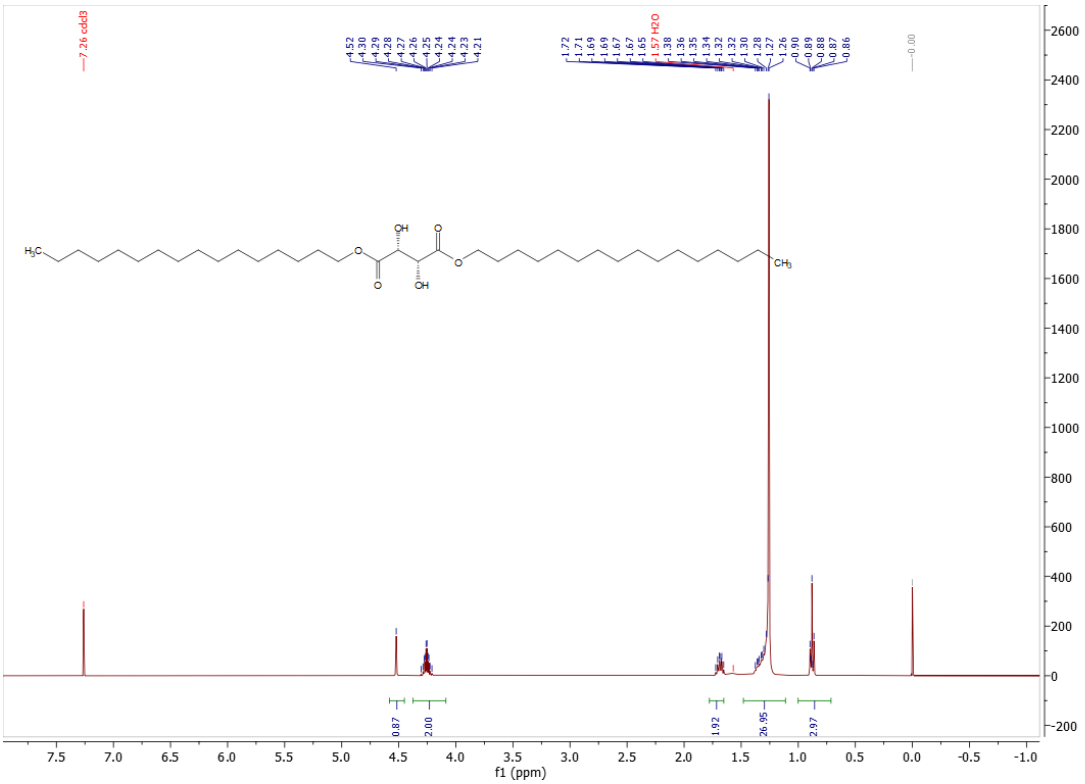

Figure S 3 ^{1}HNMR spectrum of (R,R)-di-n-hexadecyltartrate

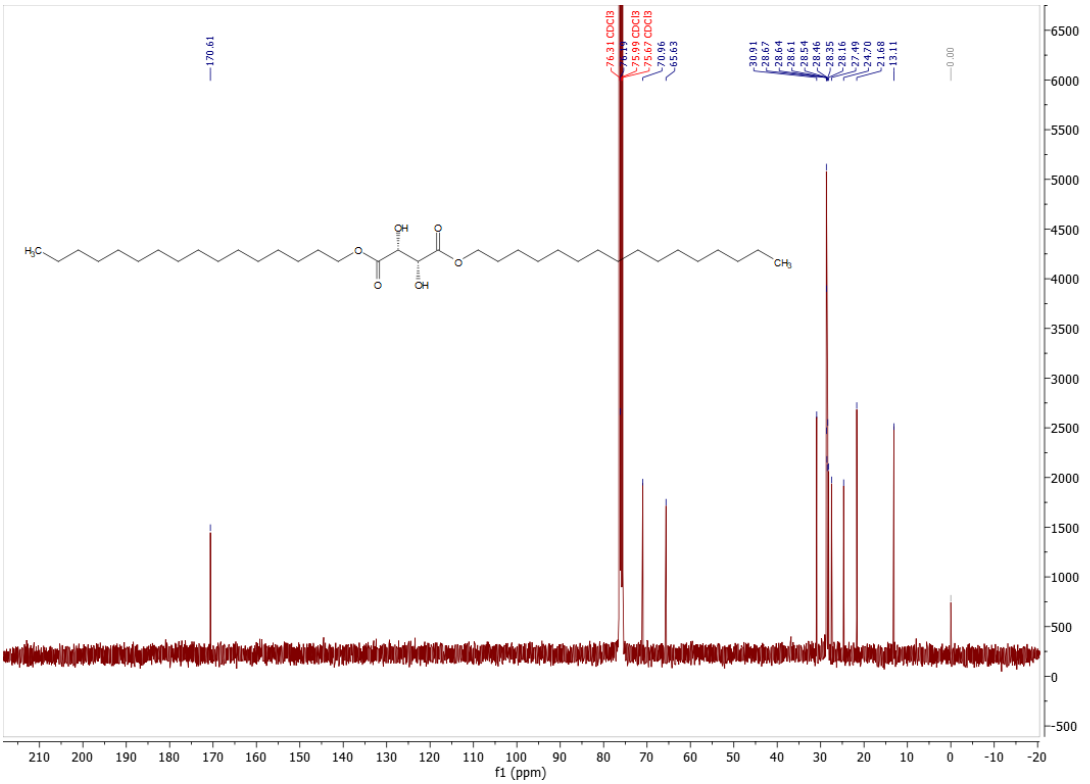

Figure S 4 ^{13}CNMR spectrum of (R,R)-di-n-hexadecyltartrate

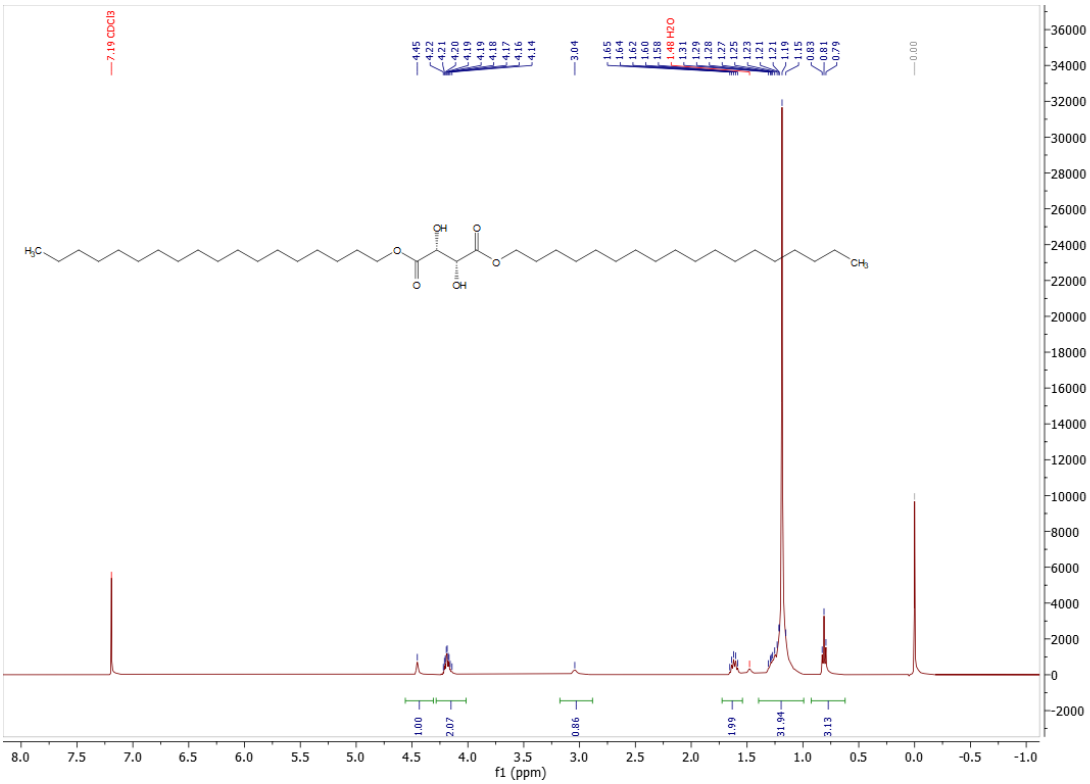

Figure S 5 ^{1}HNMR spectrum of (R,R)-di-n-octadecyltartrate

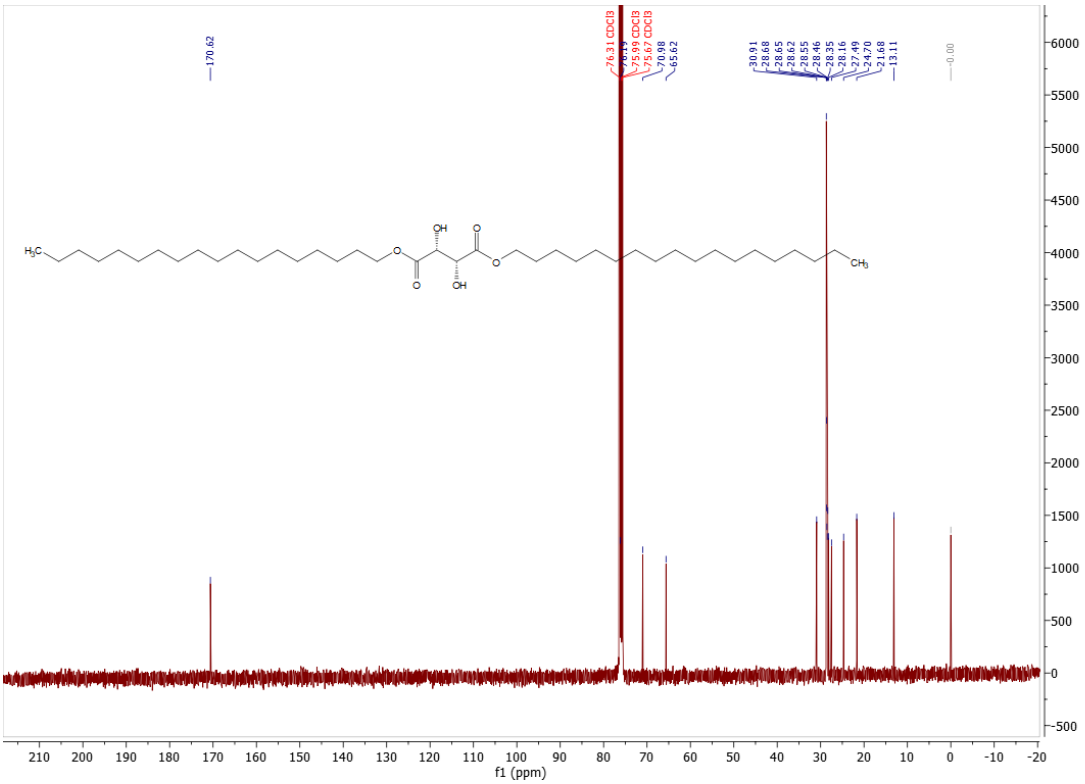

Figure S 6 [13]CNMR spectrum of (R,R)-di-n-octadecyltartrate

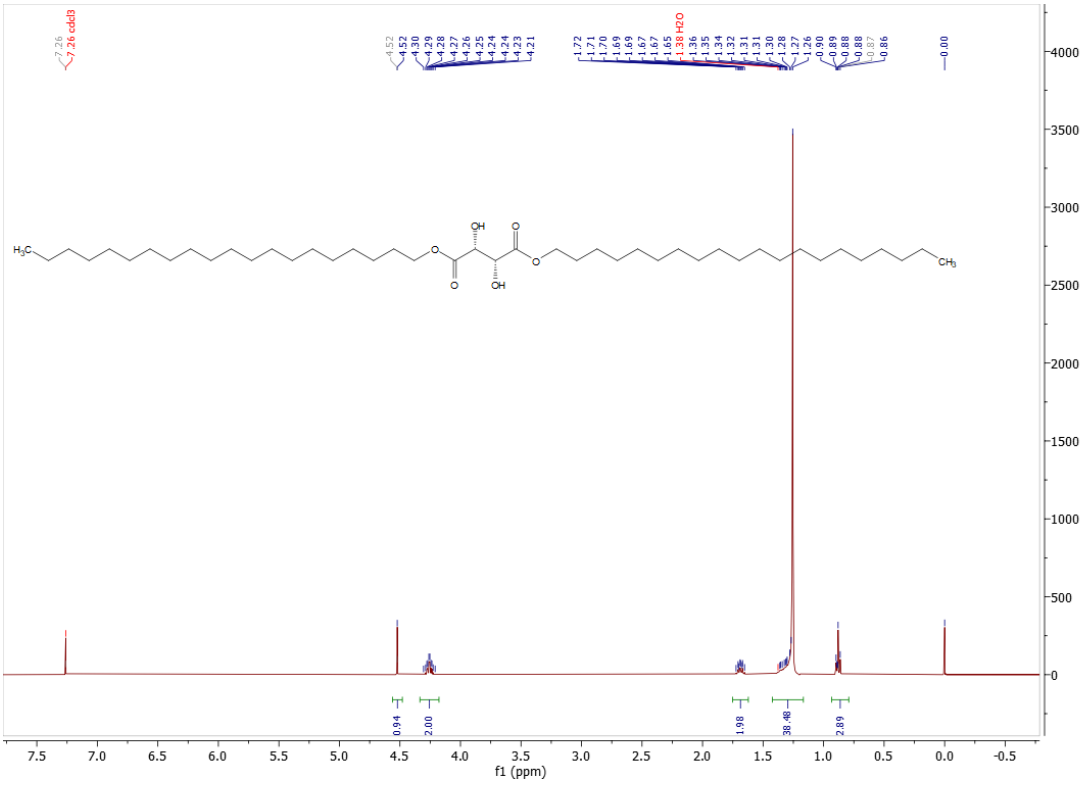

Figure S 7 [1]HNMR spectrum of (R,R)-di-n-docanosyltartrate

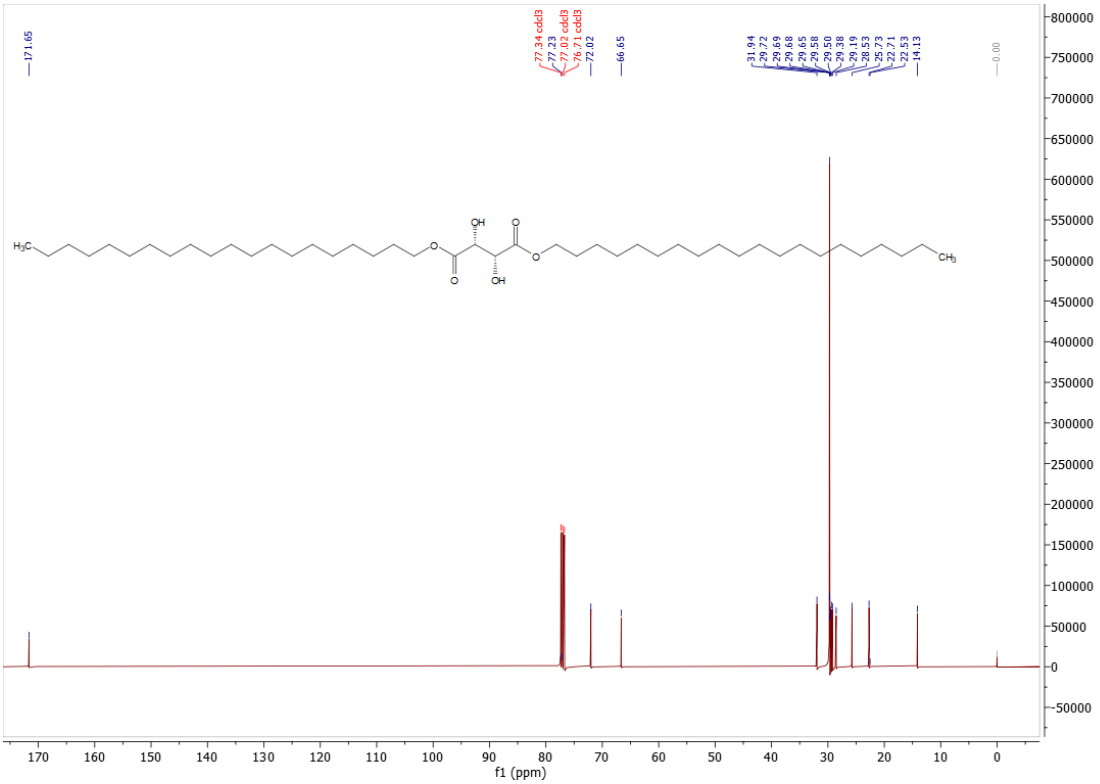

Figure S 8 [13]CNMR spectrum of (R,R)-di-n-docanosyltartrate

Mucic acid series

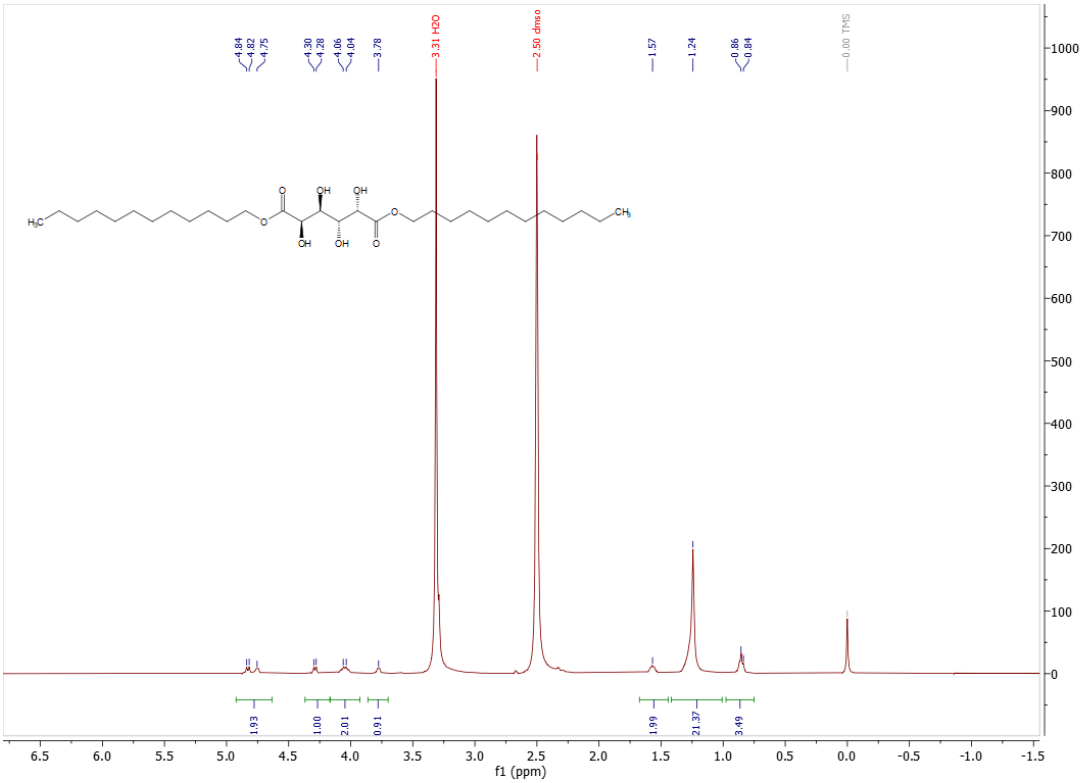

Figure S 9 [1]HNMR spectrum of di-n-laurylmucate

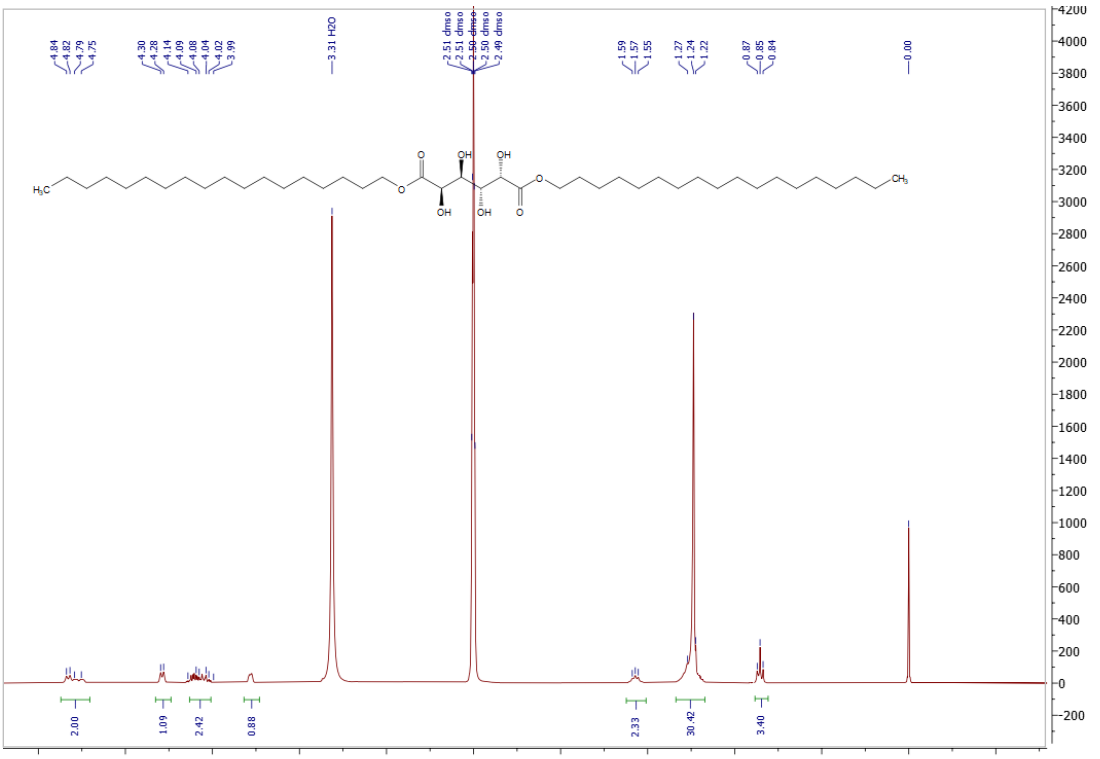

Figure S 10 [1]HNMR spectrum of di-n-stearylmucate

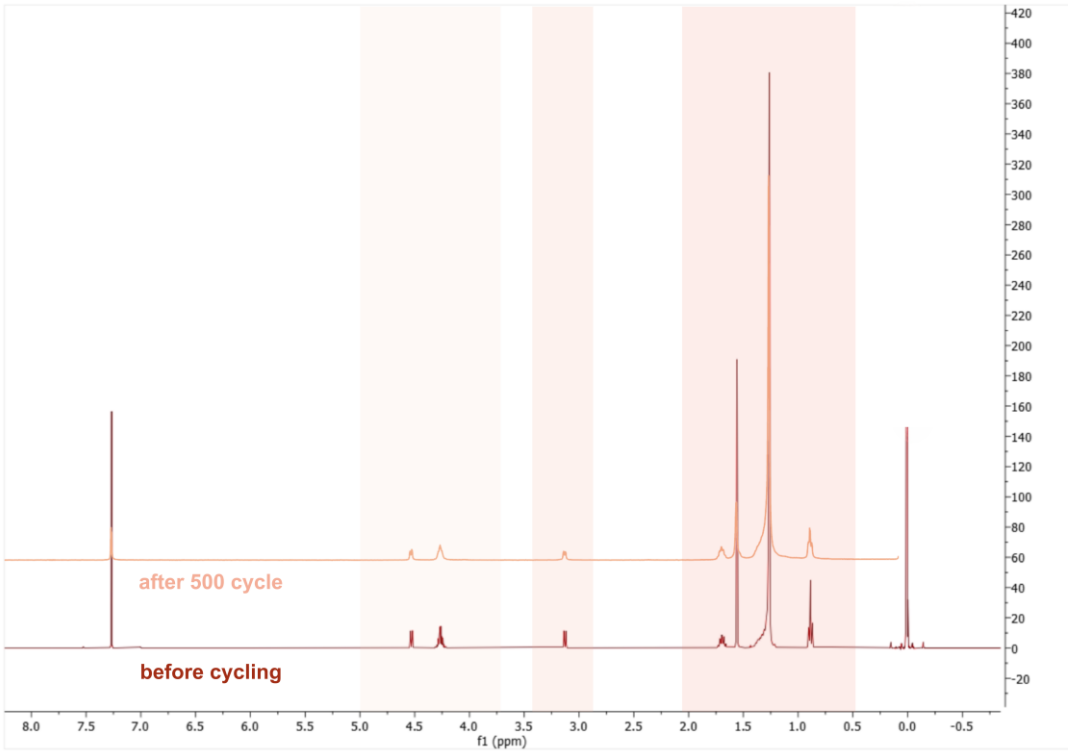

Figure S 11 [1]HNMR spectra of C18_TA_C18 before and after 500 th cycles

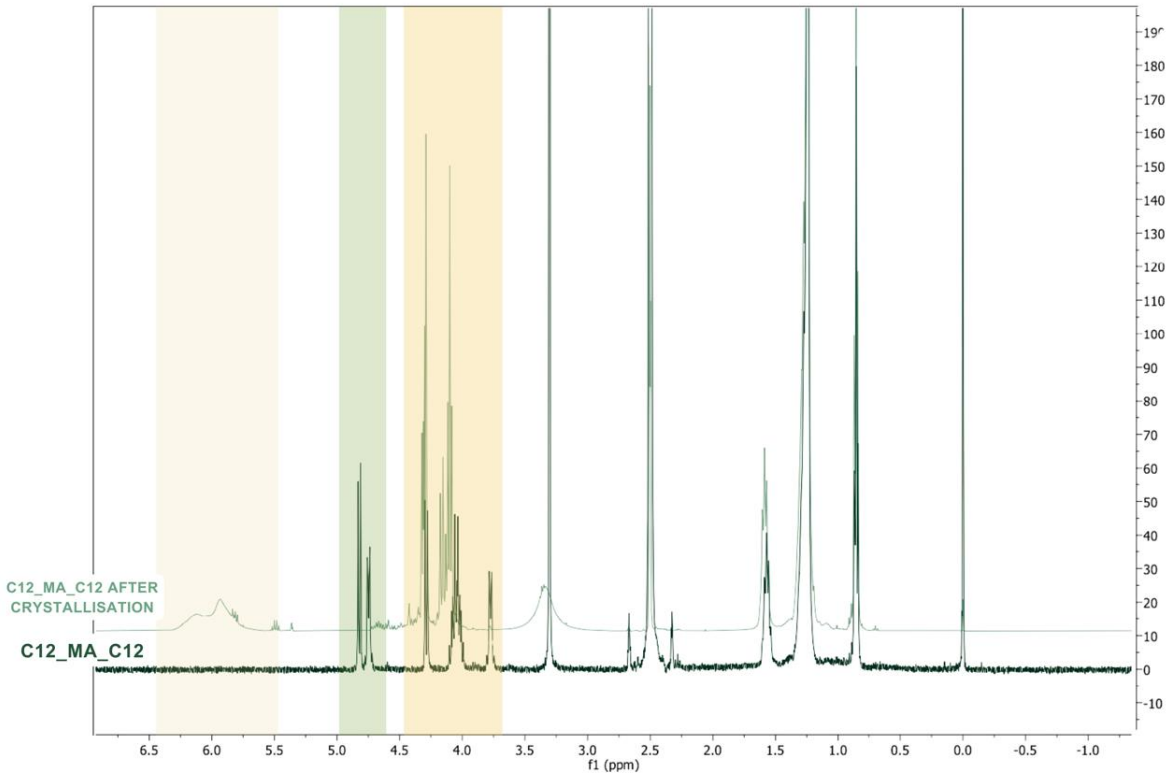

Figure S 12 Comparison of C12_MA_C12 ^{1}H NMR spectra before and after melting

TGA

Tartaric acid series

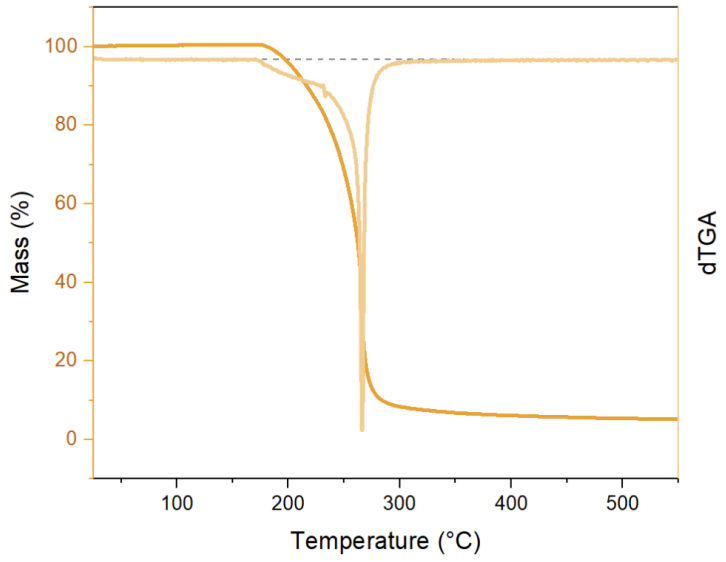

Figure S 13 TGA of L (+)-Tartaric Acid

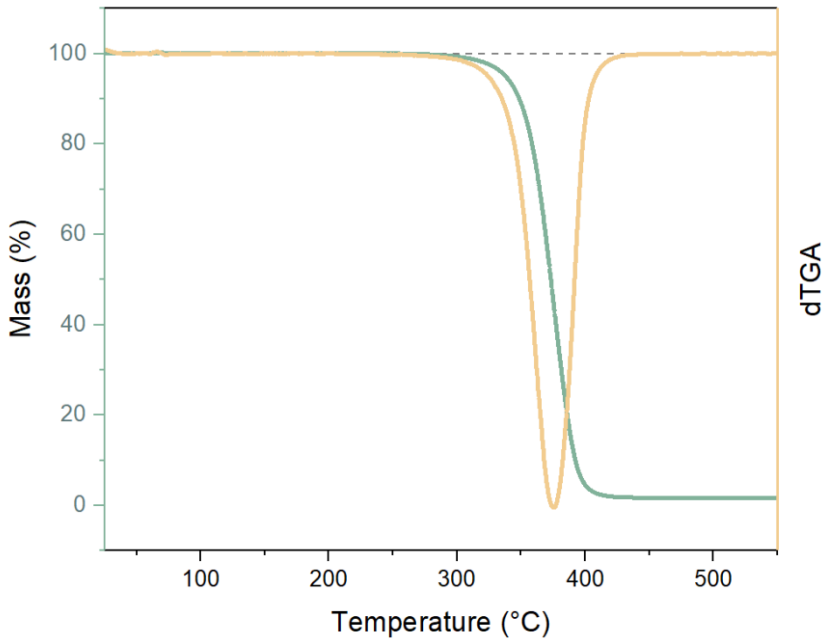

Figure S 14 TGA of (R,R)-di-n-dodecyltartrate

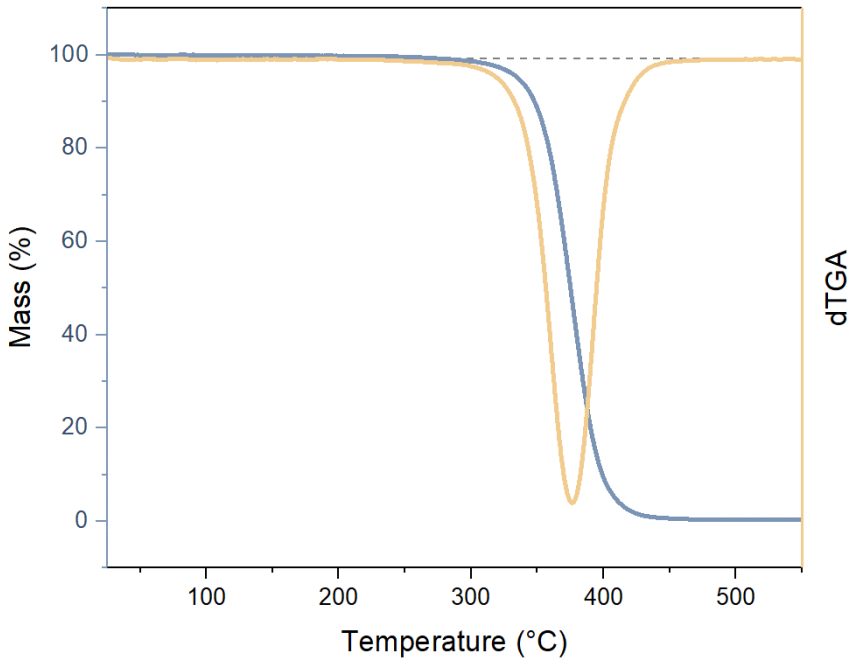

Figure S 15 TGA of (R,R)-di-n-hexadecyltartrate

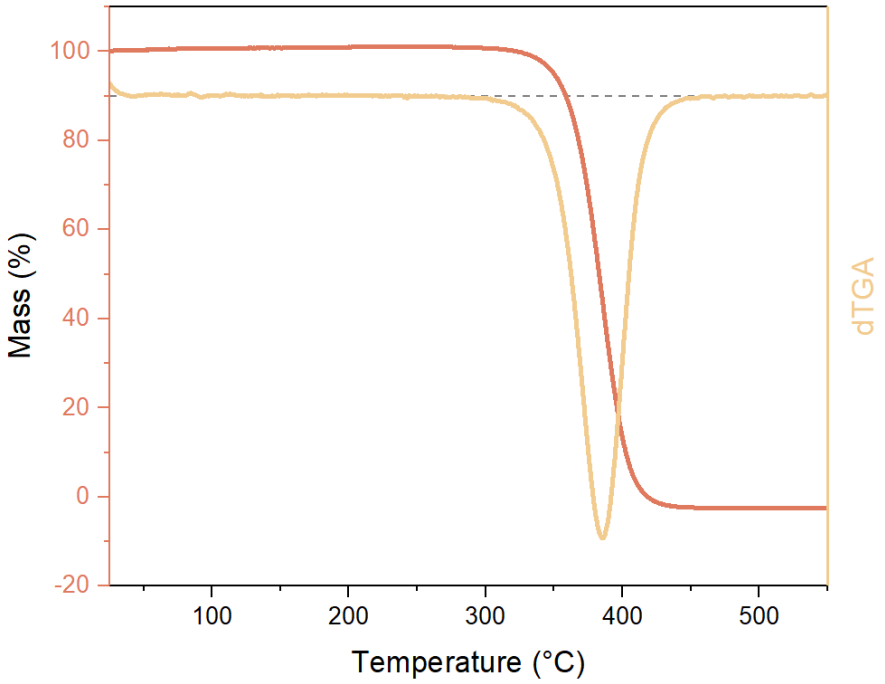

Figure S 16 TGA of (R,R)-di-n-octadecyltartrate

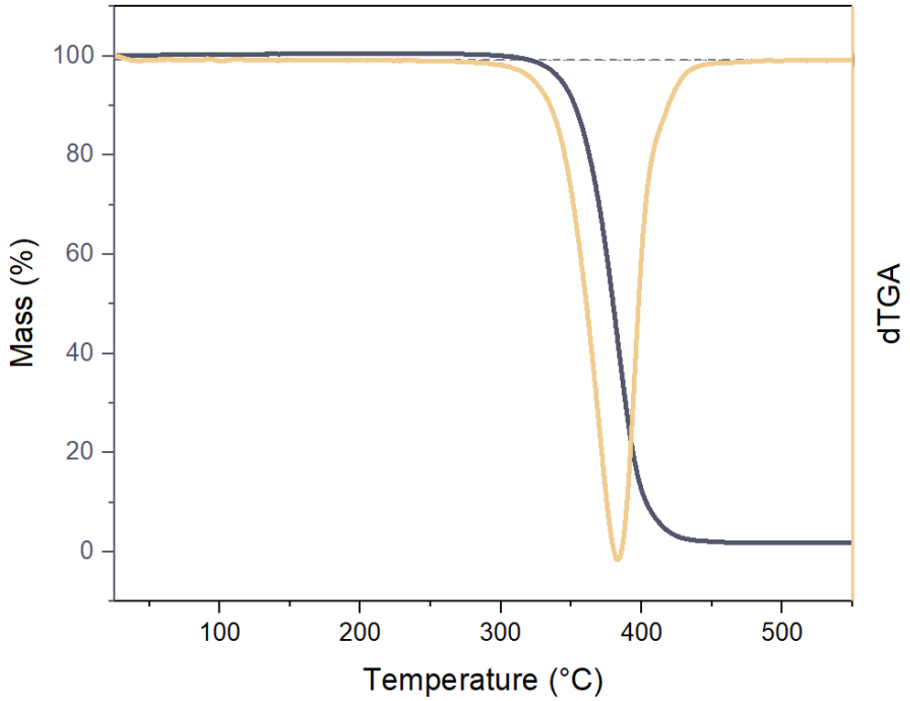

Figure S 17 TGA of (R,R)-di-n-docanosyltartrate

Mucic acid series

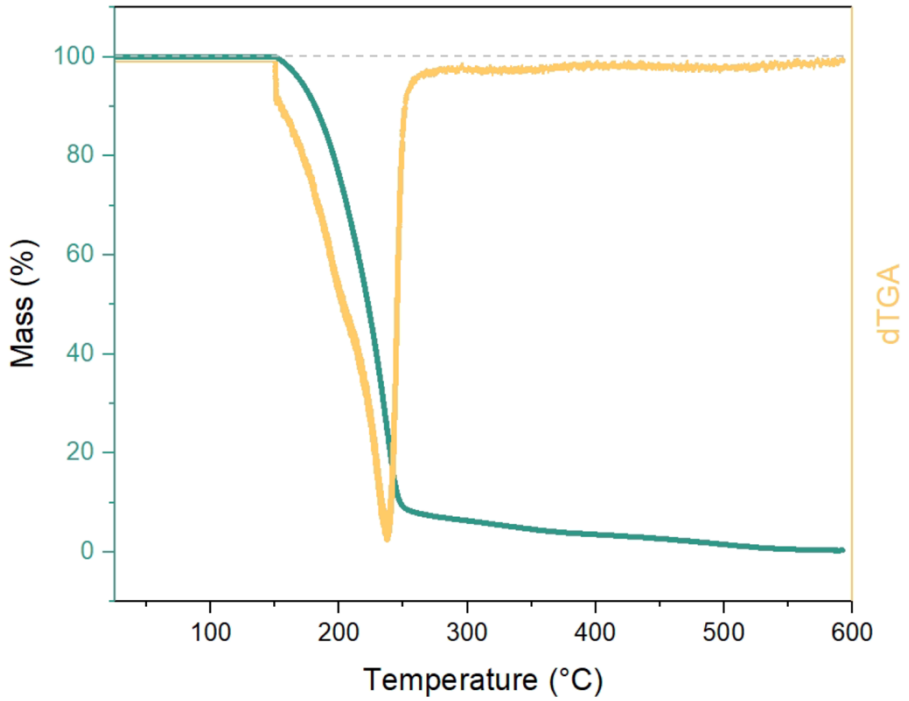

Figure S 18 TGA of di-n-hexadecylmucate

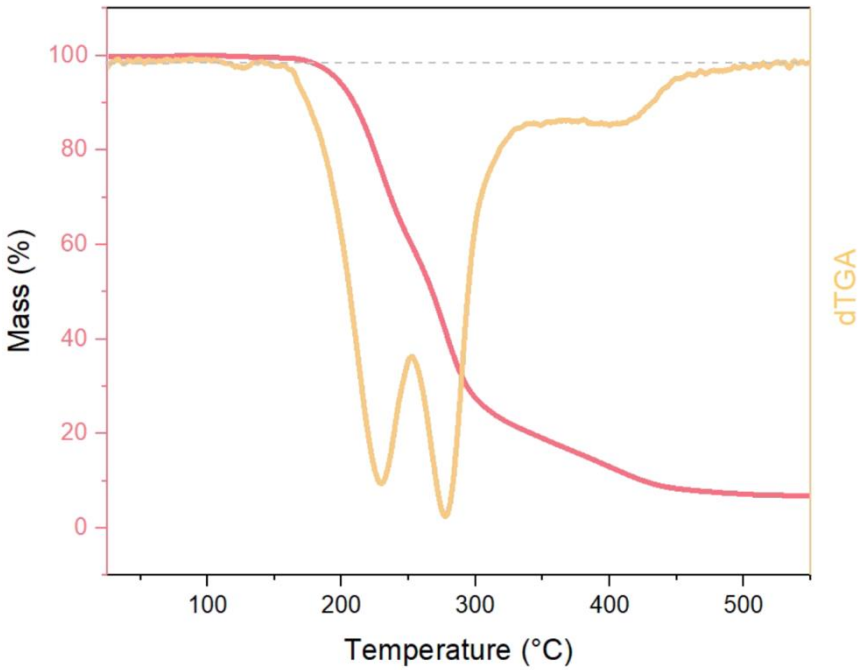

Figure S 19 TGA of di-n-octadecylmucate

DSC

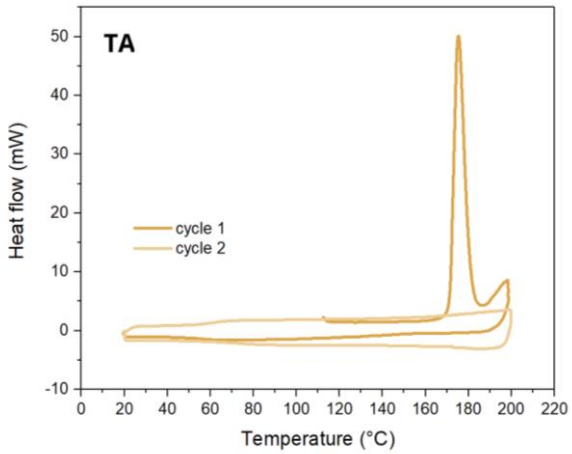

Figure S 20 DSC curve of L(+) - Tartaric Acid

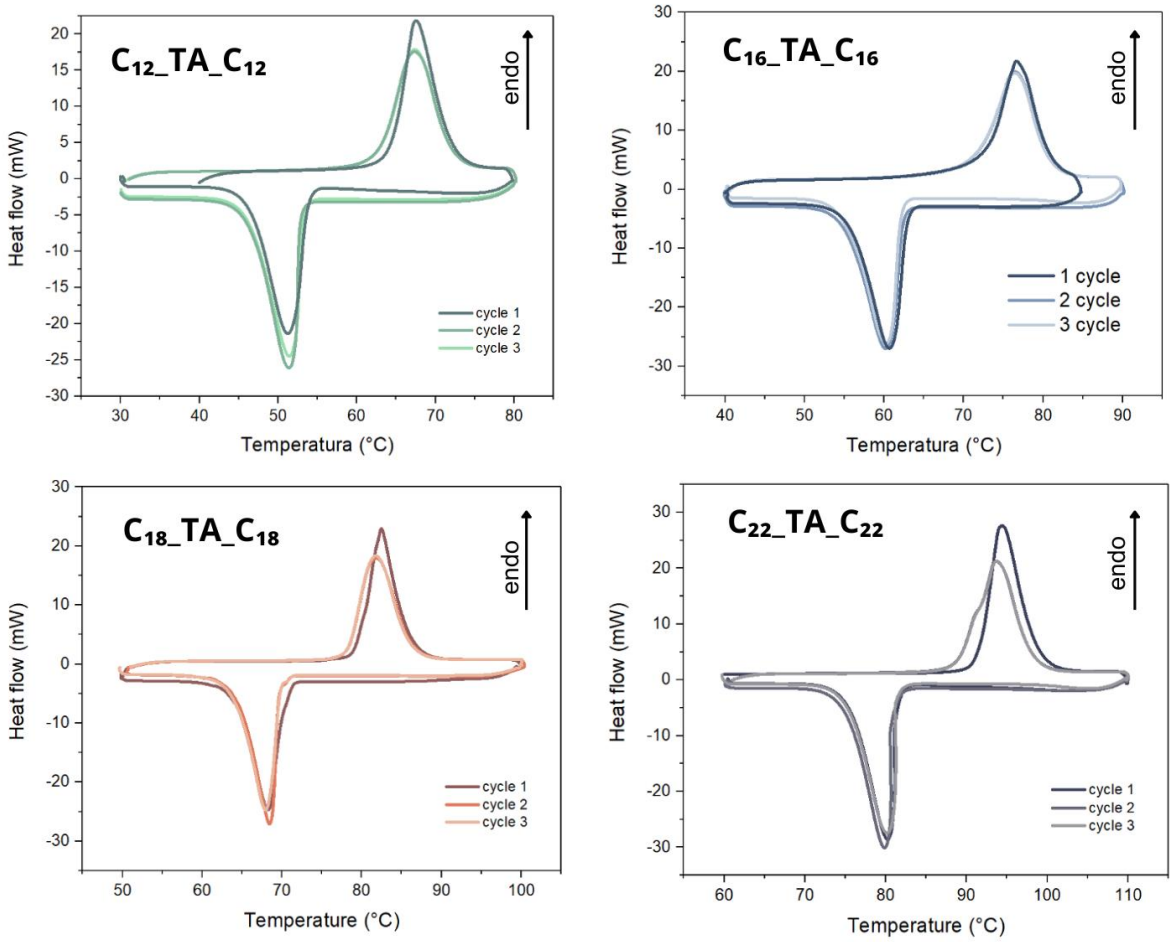

Figure S 21 DSC curves of tartaric acid diester series

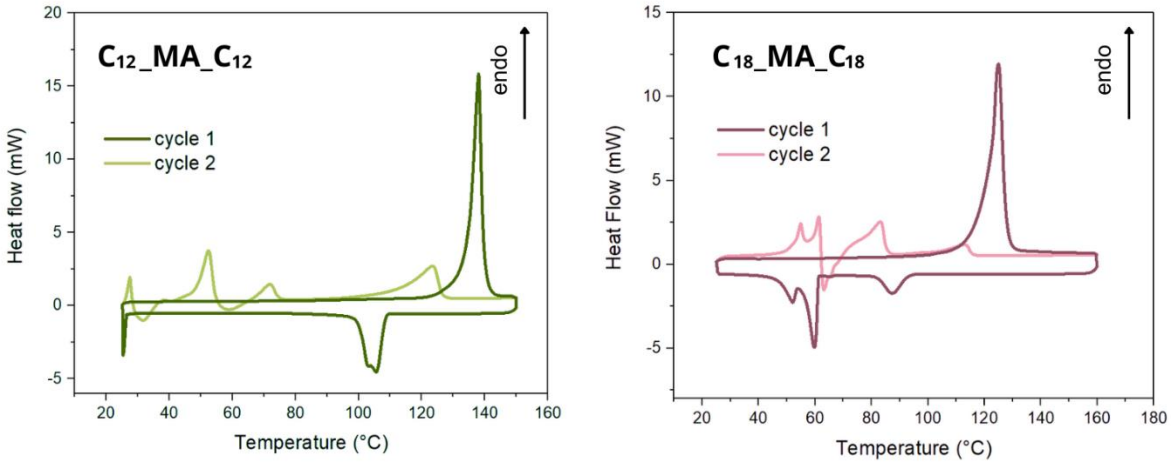

Figure S 22 DSC curves of mucic acid diester series

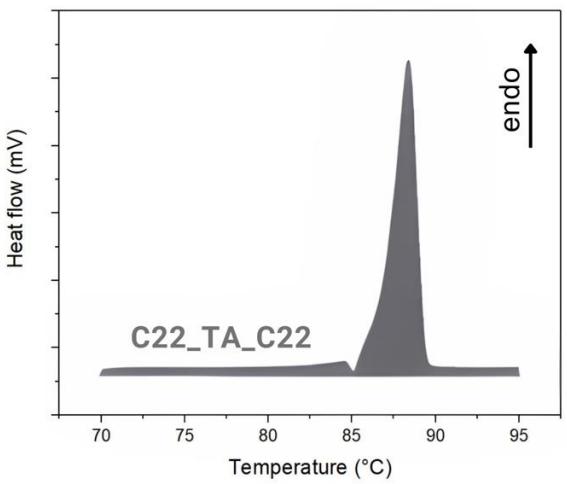

Figure S 23 DSC curve of C22_TA_C22, at a ramp rate 1° min^{-1}

FTIR

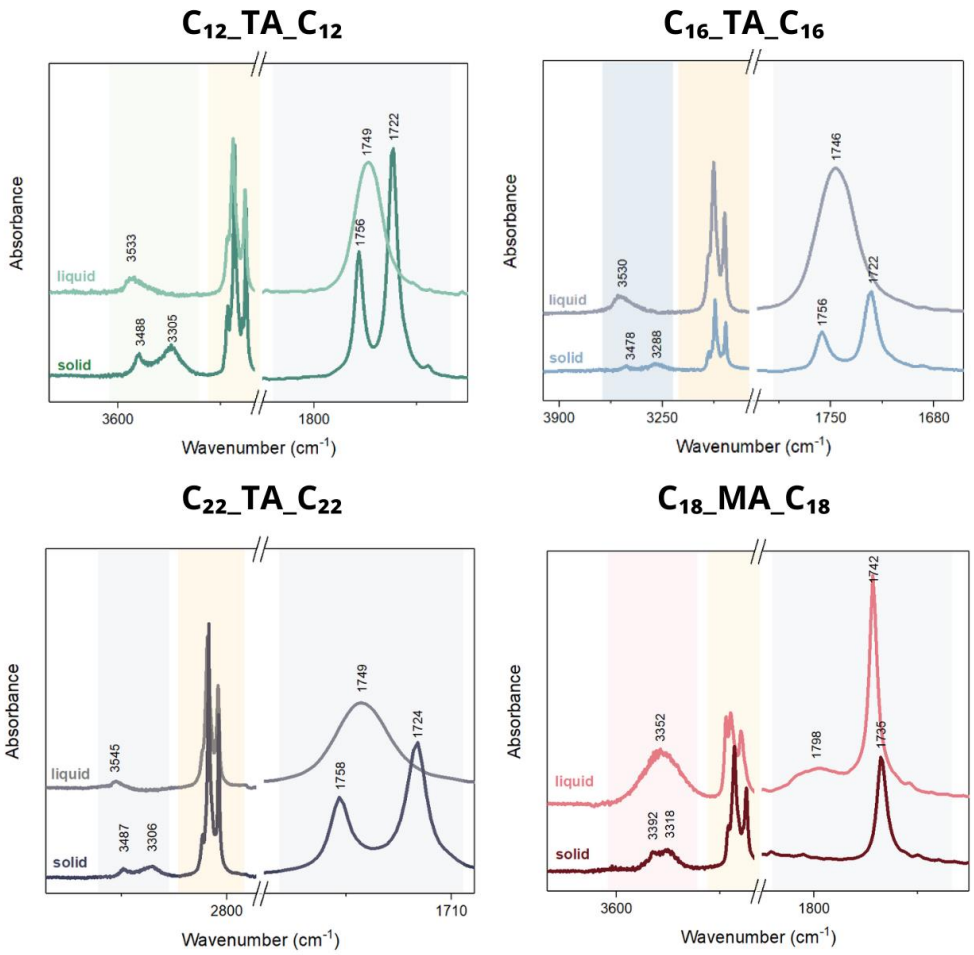

Figure S 24 FT-IR analysis of tartaric acid and mucic acid diester series in solid and liquid state

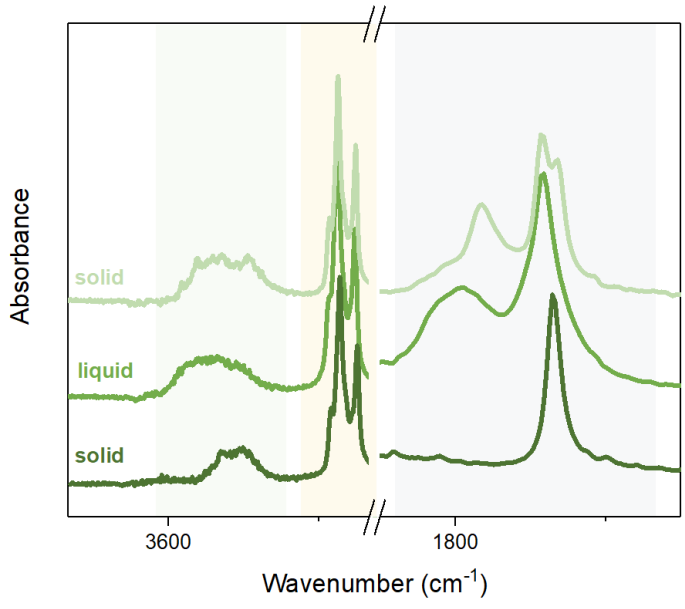

Figure S 25 FT-IR analysis of C12_MA_C12

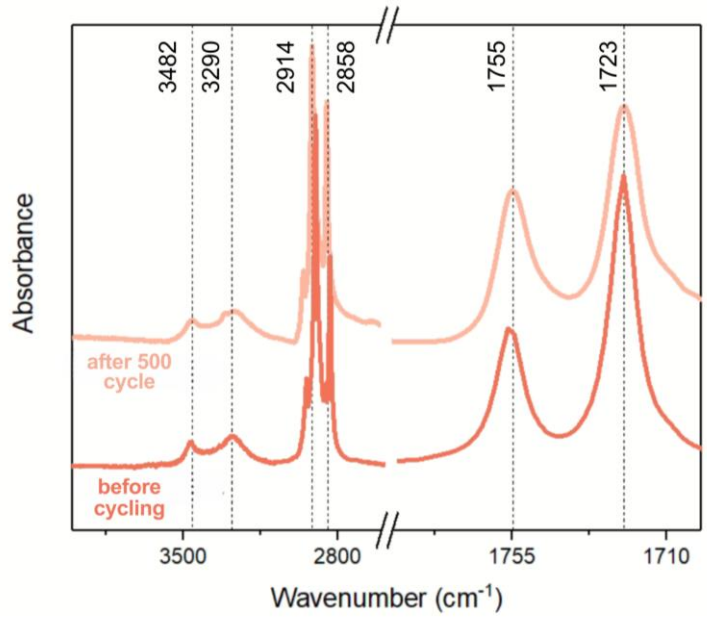

Figure S 26 FT-IR analysis of C18_TA_C18 before and after 500 th cycles

X-ray Crystallography

Extended crystal packing

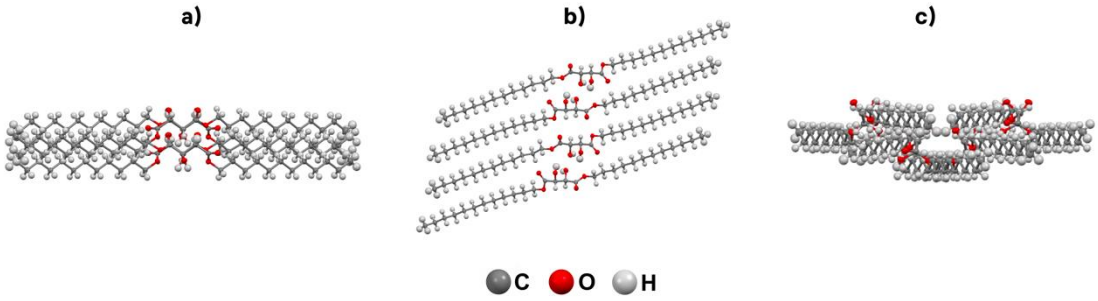

Figure S 27 Extended crystal packing of C12_TA_C12 down the a (a), b (b), c (c) axis

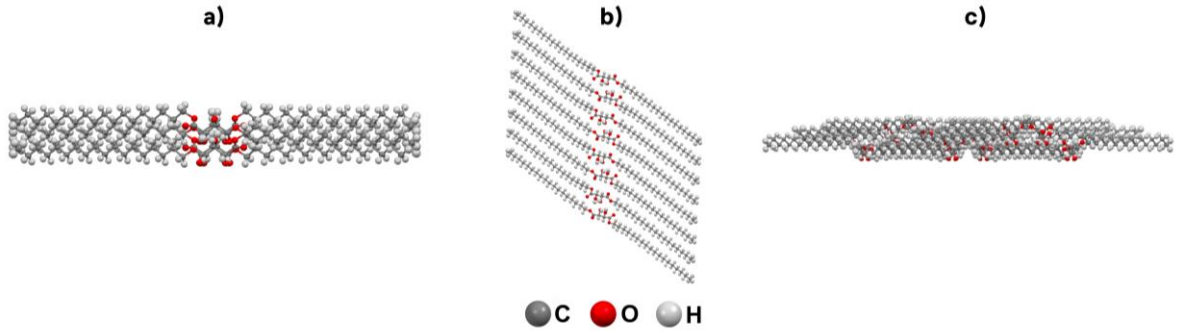

Figure S 28 Extended crystal packing of C18_TA_C18 down the a (a), b (b), c (c) axis

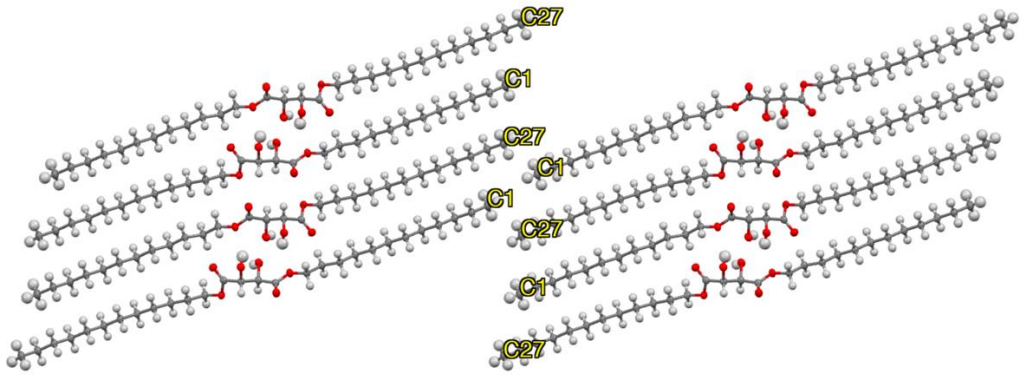

Figure S 29 Extended crystal packing of C12_TA_C12 down the b axis

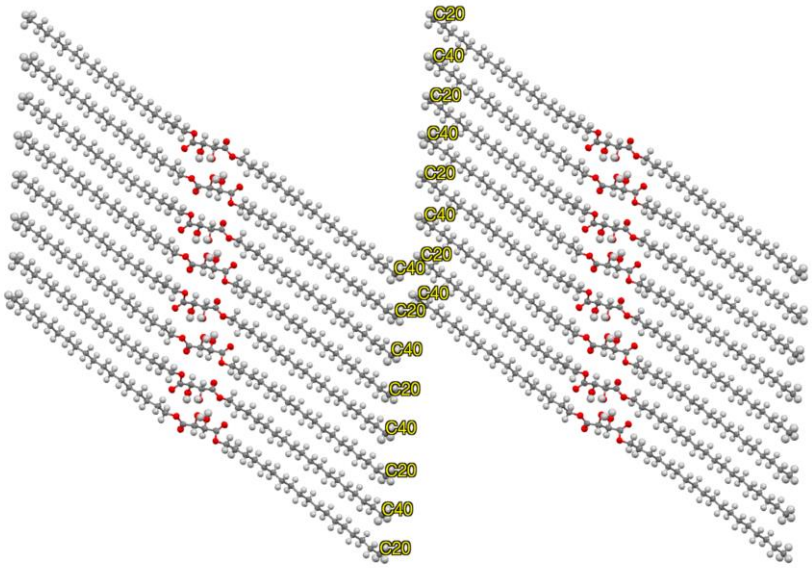

Figure S 30 Extended crystal packing of C18_TA_C18 down the b axis

Crystal data and refinement details

Table S 1 Crystal data and structure refinement for C_{12}_TA_C_{12} and C_{18}_TA_C_{18}

Identification code	**C_{12}_TA_C_{12}**	**C_{18}_TA_C_{18}**
Empirical formula	$C_{28}H_{54}O_6$	$C_{40}H_{78}O_6$
Formula weight	486.737	655.02
Temperature	-	293(2)
Crystal system	monoclinic	monoclinic
Space group	C2	C2
a/Å	17.492(4)	18.197(4)
b/Å	4.754(1)	4.7630(10)
c/Å	34.846(7)	45.953(9)
α/°	90	90
β/°	98.42(3)	93.13(3)
γ/°	90	90
Volume/Å^3	2866.5(10)	3976.9(14)
Z	1	4
ρ_{calc}g/cm^3	1.128	1.094
μ/mm^{-1}	0.077	0.071
F(000)	1080.7	1464.0
Radiation	Mo Kα (λ = 0.71073)	MoKα (λ = 0.71073)
2Θ range for data collection/°	3.54 to 64.4	0.888 to 49.998
Index ranges	$-24 \le h \le 24$, $-6 \le k \le 6$, $-46 \le l \le 46$	$-21 \le h \le 21$, $-5 \le k \le 5$, $-54 \le l \le 54$
Reflections collected	23610	21441
Independent reflections	8137 [R_{int} = 0.1179, R_{sigma} = 0.1106]	6683 [R_{int} = 0.1003, R_{sigma} = 0.0928]
Data/restraints/parameters	8137/3/317	6683/1/419
Goodness-of-fit on F^2	0.997	1.060
Final R indexes [I>=2σ (I)]	R_1 = 0.0858, wR_2 = 0.2103	R_1 = 0.0812, wR_2 = 0.2300
Final R indexes [all data]	R_1 = 0.0902, wR_2 = 0.2201	R_1 = 0.1170, wR_2 = 0.2764
Largest diff. peak/hole / e Å^{-3}	0.46/-0.74	0.47/-0.39
Flack parameter	-0.0(6)	1.2(10)

Hydrogen bond tables generated from Olex2

Table S 2 Distance and angles of strong hydrogen bond in C_{12}_TA_C_{12}

C_{12}_TA_C_{12}						
D	**H**	**A**	**D-H length [Å]**	**H···A length [Å]**	**D-H···A length [Å]**	**D-H···A angle [°]**
O4	H3	O3	0.83(2)	1.81(2)	2.64(2)	174(2)
O3	H4	O4	0.89(3)	2.21(3)	2.83(18)	126(3)
Average			0.86	2.01	2.74	150

Table S 3 Distance and angles of strong hydrogen bond in C_{18}_TA_C_{18}

C_{18}_TA_C_{18}						
D	**H**	**A**	**D-H length [Å]**	**H···A length [Å]**	**D-H···A length [Å]**	**D-H···A angle [°]**
O1	H1	O4	0.82	2.23	2.79	123
O4	H4	O1	0.82	1.83	2.63	168
Average			0.82	2.03	2.71	146

Distances and angles of hydrogen bonds calculated through the Mercury 2021.2.0 software

Table S 4 Distance and angles of hydrogen bond in C_{12}_TA_C_{12}

C_{12}_TA_C_{12}						
D	**H**	**A**	**D-H length [Å]**	**H···A length [Å]**	**D-H···A length [Å]**	**D-H···A angle [°]**
O4	H4	O1	0.89	2.57	3.07	116
C14	H14	O2	0.98	2.63	3.34	129
C15	H15		0.98	2.58	3.49	155
C16	H16b		0.97	2.52	3.28	135
O4	H3	O3	0.83	1.81	2.64	174
O3	H4	O4	0.89	2.21	2.82	126
C10	H10b	O5	0.97	2.54	3.31	136
C11	H11a		0.97	2.67	3.55	148
C12	H12a		0.97	2.50	3.25	134
Average			0.93	2.60	3.34	139

Table S 5 Distance and angles of hydrogen bond in C_{18}_TA_C_{18}

C_{18}_TA_C_{18}						
D	**H**	**A**	**D-H length [Å]**	**H···A length [Å]**	**D-H···A length [Å]**	**D-H···A angle [°]**
O4	H4	O1	0.82	1.83	2.63	168
C23	H23B	O2	0.97	2.51	3.27	135
C24	H24A		0.97	2.67	3.54	147
C25	H25B		0.97	2.61	3.38	136
O1	H1	O4	0.82	2.23	2.79	123
O4	H4	O4’	0.82	2.65	3.07	114
C3	H3A	O5	0.97	2.41	3.24	144
C21	H21		0.98	2.65	3.34	128
O1	H1	O6	0.82	2.62	3.13	122
Average			0.94	2.75	3.13	135

Hirshfeld surface interactions breakdown

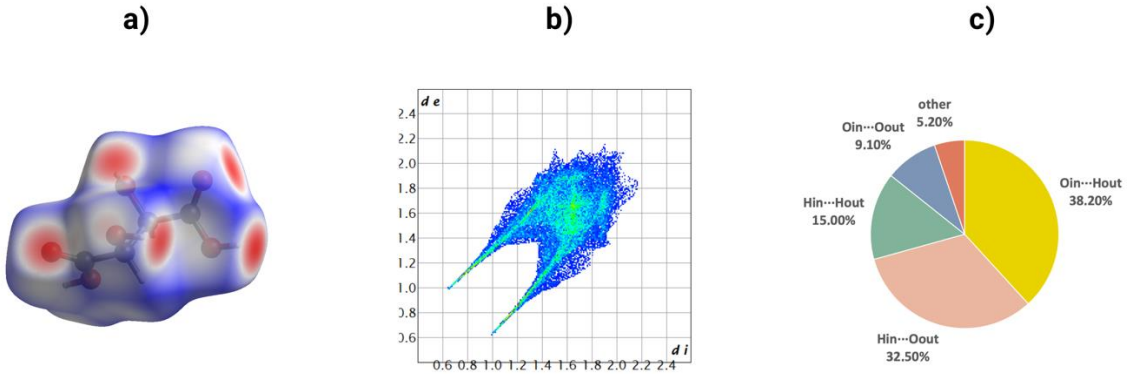

Figure S 31 Hirshfeld surface interactions breakdown for TA. a) 3D Hirshfeld surface b) fingerplot c) percentage of interactions.

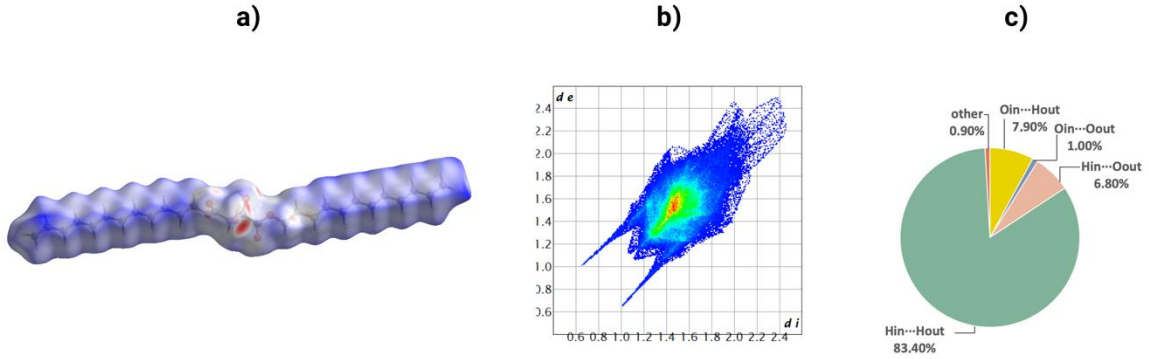

Figure S 32 Hirshfeld surface interactions breakdown for C_{12}_TA_C_{12}. a) 3D Hirshfeld surface b) fingerplot c) percentage of interactions.

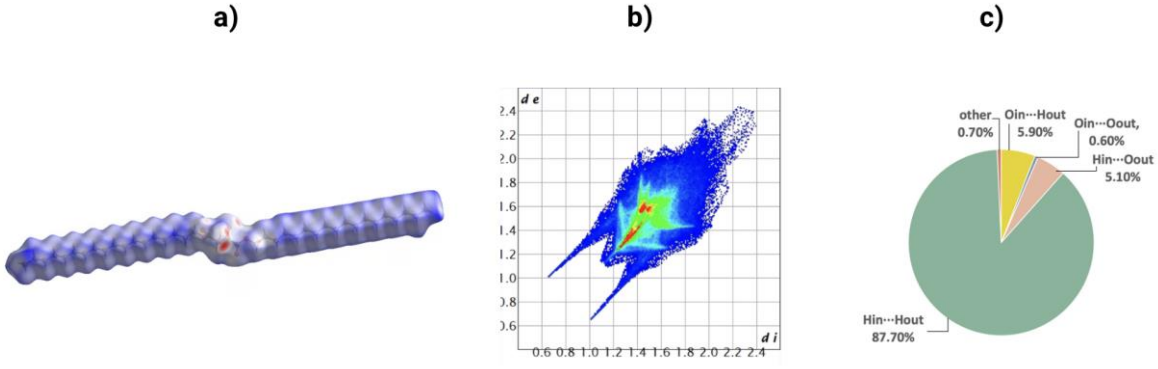

Figure S 33 Hirshfeld surface interactions breakdown for C18_TA_C18. a) 3D Hirshfeld surface b) fingerplot c) percentage of interactions.

Table S 6 The state of the art presenting organic PCMs.

Compound	T_m	ΔH_f	Biorenewable origin	Ref.
Myristic acid	53	181	✓	1
Palmitic acid	61	198		
Stearinic acid	69	202		
1-hexadecanol	49	237	✓	2
1-octadecanol	57	248		
Glycerol tristearate	64	149	✓	3
Glycerol tripalmitate	59	186		
Glyceriol tribehenate	82	214		4
Erythritol tetrapalmitate	22	201	✓	5
Xylitol pentastearate	32	205		6
Galactitol hexastearate	50	251		7

Decyl eicosanate	41	232	✓	[8]
Tetradecyl octadecanoate	49	222	✓	[9]
Tetradecyl eicosanoate	53	201		
Hexadecyl eicosanate	59	226	✓	[10]
Octadecyl eicosanate	65	226	✓	[11]
Cutina AGS	60	213	✓	[12]
Dihexadecyl-1,10-decanedioate	58	214	✓	[13]
Dihexadecyl-1,8- octanedioate	55	216	✓	[14]
N-octadecylstearamide	95	155	✗	[15]
N-hexadecyl-decanamide	79	201	✗	[15]
1-(Decyl sulfonyl) decane	89	204	✗	[16]
Nonacosane	63	240	✗	[17]
Tetratriacontane	76	269	✗	[17]
C_{18}_TA_C_{18}	82	221	✓	this work
C_{22}_TA_C_{22}	94	203	✓	this work

Literature

1 N. Wan, Y.-Y. Jia, Y.-L. Hou, X.-X. Ma, Y.-S. He, C. Li, S.-Y. Zhou and B.-L. Zhang, *Preparation, Physicochemical Properties, and Transfection Activities of Tartaric Acid-Based Cationic Lipids as Effective Nonviral Gene Delivery Vectors*, 1112, vol. 39.

2 J.F. Carson, *J Am Chem Soc*.

3 A. Sari, *Energy Convers Manag*, 2003, **44**, 2277–2287.

4 Q. Zhang, H. Yan, Z. Zhang, J. Luo, N. Yin, Z. Tan and Q. Shi, *Materials Today Sustainability*, 2021, **11–12**, 100064.

5 A. Sar, A. Bier, A. Karaipekli, C. Alkan and A. Karadag, *Solar Energy Materials and Solar Cells*, 2010, **94**, 1711–1715.

6 C. K. Zéberg-Mikkelsen and E. H. Stenby, *Fluid Phase Equilib*, 1999, **162**, 7–17.

7 A. Sari, R. Eroglu, A. Biçer and A. Karaipekli, *Chem Eng Technol*, 2011, **34**, 87–92.

8 A. Biçer and A. Sar, *Solar Energy Materials and Solar Cells*, 2012, **102**, 125–130.

9 A. Sari, A. Biçer, Ö. Lafçi and M. Ceylan, *Solar Energy*, 2011, **85**, 2061–2071.

10 R. Ravotti, O. Fellmann, N. Lardon, L. J. Fischer, A. Stamatiou and J. Worlitschek, *Appl. Sci.,* 2019, ***9*(2)**, 225

11 A. A. Aydn and H. Okutan, *Solar Energy Materials and Solar Cells*, 2011, **95**, 2752–2762.

12 A. A. Aydin and A. Aydin, *Solar Energy Materials and Solar Cells*, 2012, **96**, 93–100.

13 A. Alper Aydn, *Solar Energy Materials and Solar Cells*, 2013, **113**, 44–51.

14 A. A. Aydn, *Solar Energy Materials and Solar Cells*, 2013, **108**, 98–104.

15 A. A. Aydın and N. Çalık, *Solar Energy Materials and Solar Cells*, 2024, **269**, 112785.

16 A. A. Aydın and G. Toprakçı, *Solar Energy Materials and Solar Cells*, 2021, **220**, 110822.